

Some aspects of the phase diagram of double-exchange systems

Daniel P. Arovas

Department of Physics, University of California at San Diego, La Jolla, California 92093

Francisco Guinea

Department of Physics, University of California at San Diego, La Jolla, California 92093

and Instituto de Ciencia de Materiales, Consejo Superior de Investigaciones Científicas, Cantoblanco, 28049 Madrid, Spain

(Received 26 November 1997)

The phase diagram of doped manganate compounds $\text{La}_{1-x}\text{A}_x\text{MnO}_3$ (with divalent A) with small x is studied. We analyze an extension of the double-exchange model using the Schwinger boson formalism. Earlier work by de Gennes on the existence of a canted phase is reproduced, although this phase is shown to be unstable towards phase separation in a broad regime of physical interest. We numerically solve the mean-field equations for our model and exhibit its phase diagrams.

[S0163-1829(98)01238-7]

I. INTRODUCTION

Doped manganese oxides show many unusual features, the most striking being the colossal magnetoresistance in the ferromagnetic phase.¹⁻³ The phase diagram, as a function of doping and temperature, is far from elucidated. At small dopings, many experiments are interpreted in terms of the phase diagram proposed by de Gennes,⁴ who studied the so-called double-exchange model⁵ (see below). Some experiments indeed confirm the predictions derived from this approach.⁶ Others, however, seem to imply a more complex behavior, including charge ordering^{7,8} or coexisting phases.^{9,10} In addition, these materials show a metal-insulator transition at low dopings and low temperatures.¹¹

In the following, we will analyze the phase diagram of these systems using the Schwinger boson representation¹² for the magnetic moments, which are described by the double-exchange model. We neglect the role of lattice distortions, which may be important at high dopings, where the Jahn-Teller distortion present in undoped systems disappears.¹³ The scheme that we use allows us to obtain a description of the spin waves. In more conventional systems, it has been shown that quantum and thermal fluctuations are adequately described^{12,14} in this approach. The method has already been used to study the quasiparticle coherence in the manganese oxides.¹⁵ Finally, the calculations reported here reproduce the work of de Gennes⁴ in the zero-temperature, large- S limit. The general features of the model are described in the next section. Sections III and IV adapt the Schwinger boson method to the double-exchange model. The results for $T=0$ are presented in Sec. V, where the relation of our work to the original calculation by de Gennes⁴ is discussed. Section VI is devoted to finite-temperature results. Finally, Sec. VII contains a discussion of experimental results and related theoretical work.

II. MODEL

In materials such as $\text{La}_{1-x}\text{A}_x\text{MnO}_3$ (with A divalent), a fraction x of Mn ions are in $3d^3$ (Mn^{4+}) configurations, with

the remaining fraction $1-x$ in $3d^4$ (Mn^{3+}) states. In a cubic crystal field, the Mn $3d$ levels split into a lower t_{2g} triplet and an upper e_g doublet. Intra-atomic ("Hund's rules") couplings overwhelm the crystal-field splitting, hence the t_{2g} levels are always triply occupied and form a $S=\frac{3}{2}$ "core spin." In Mn^{3+} ions, the e_g orbitals are further split by a static Jahn-Teller (JT) distortion, which, together with the Hund's rules, completely determines both the orbital as well as spin state of the e_g electron. The e_g electrons may be represented by spinless, single-orbital fermions whose hopping is modulated by the overlap of the core-spin wave functions. If we treat the core spin on site i using the Schwinger representation, $\mathbf{S}_i = \frac{1}{2} b_{i\alpha}^\dagger \boldsymbol{\sigma}_{\alpha\beta} b_{i\beta}$ ($\alpha, \beta = \uparrow, \downarrow$, $\sum_\alpha b_{i\alpha}^\dagger b_{i\alpha} = 2S$), then the e_g hole creation operator $\psi_{i\sigma}^\dagger$ may be factored into a spinless fermion c and the Schwinger boson $b_{i\sigma}$ that supply the core-spin orientation: $\psi_{i\sigma}^\dagger = c_i^\dagger b_{i\sigma}$. The role of the core-spin overlap to electron hopping in these materials is widely appreciated (see, e.g., Refs. 4, 13, 15, and 16).

Neighboring core spins are coupled via superexchange through the O $2p$ orbitals.^{2,17} For pure LaMnO_3 ($x=0$), the c -axis exchange is antiferromagnetic while the exchange between neighboring ions in a plane perpendicular to \hat{c} is ferromagnetic. We have therefore chosen to study the model defined by the Hamiltonian²¹

$$\mathcal{H} = -\frac{1}{2} S \sum_{\langle ij \rangle, \sigma} [t_{ij} c_i^\dagger c_j b_{i\sigma} b_{j\sigma}^\dagger + \text{H.c.}] - \sum_{\langle ij \rangle} J_{ij} \mathbf{S}_i \cdot \mathbf{S}_j \quad (1)$$

for a cubic lattice of Mn ions, where the exchange $J_{ij} = -J_v < 0$ along vertical links and $J_{ij} = J_h > 0$ along horizontal links. The coexistence of in-plane ferromagnetic and out-of-plane antiferromagnetic interactions is due to the presence of the Jahn-Teller distortions, which modulate the possible transitions between filled and empty e_g orbitals.¹⁷ Experiments suggest $J_v \approx J_h \approx 0.58$ meV.^{18,19} The parameters t_{ij} describe the hopping between e_g orbitals. Note that, when the core spin in neighboring sites is aligned, the effective hopping is given by $S^2 t_{ij} \approx 100$ meV, according to band-structure calculations.²⁰

The model has the unphysical feature that the exchange between core spins is fixed independent of the fermion occupancy and hence it cannot reflect the difference between Mn^{3+} - Mn^{3+} , Mn^{3+} - Mn^{4+} , and Mn^{4+} - Mn^{4+} exchange (note that Mn^{4+} - Mn^{4+} exchange, appropriate to pure CaMnO_3 , is always antiferromagnetic¹⁷). In addition, we assume a strong static JT distortion that renders the conduction orbital non-degenerate, whereas in the real materials this distortion vanishes for $x \geq 0.2$.

The model does capture what is perhaps the most important aspect of the interaction between fermions and core spins, namely, that ferromagnetic core-spin alignment leads to a larger fermion bandwidth and reduced kinetic energy. We aim to apply it in the small- x region of the phase diagram, where most of the links are between Mn^{3+} ions, so that the drawback mentioned in the preceding paragraph should not change significantly the results.

This hopping Hamiltonian itself, in the absence of Heisenberg exchange terms, was considered by Sarker,¹⁵ who found a finite-temperature transition between a ferromagnetic metal and a spin-disordered state, presumably insulating, in which the fermion band is completely incoherent.

III. MEAN-FIELD THEORY

We now devise a mean-field theory for the Hamiltonian of Eq. (1). We treat the spins using the Schwinger boson description:¹²

$$\mathbf{S}_i \cdot \mathbf{S}_j = \frac{1}{2} \mathcal{F}_{ij}^\dagger \mathcal{F}_{ij} : - S^2 = - : \frac{1}{2} \mathcal{A}_{ij}^\dagger \mathcal{A}_{ij} : + S^2, \quad (2)$$

where

$$\begin{aligned} \mathcal{F}_{ij} &= b_{i\uparrow} b_{j\uparrow}^\dagger + b_{i\downarrow} b_{j\downarrow}^\dagger, \\ \mathcal{A}_{ij} &= b_{i\uparrow} b_{j\downarrow} - b_{i\downarrow} b_{j\uparrow}, \end{aligned} \quad (3)$$

and $:\mathcal{O}:$ means normal ordering of \mathcal{O} . A Lagrange multiplier Λ_i is introduced at each site to enforce the local constraint $\sum_\alpha b_{i\alpha}^\dagger b_{i\alpha} = 2S$. Expressed in terms of bosonic and fermionic creation and annihilation operators, both the hopping and superexchange terms in \mathcal{H} are quartic.

Following Sarker,¹⁵ we invoke a Hartree-Fock decoupling of the hopping term,

$$\begin{aligned} c_i^\dagger c_j \mathcal{F}_{ij} &\rightarrow -\langle c_i^\dagger c_j \rangle \langle \mathcal{F}_{ij} \rangle + c_i^\dagger c_j \langle \mathcal{F}_{ij} \rangle + \langle c_i^\dagger c_j \rangle \mathcal{F}_{ij} \\ &+ \text{fluctuations} \end{aligned}$$

dropping the fluctuations. The Heisenberg exchange is similarly decoupled, as in Ref. 12. We assume the mean-field solution is uniform:

$$\langle \Lambda_i \rangle = \Lambda,$$

$$\langle \mathcal{F}_{ij} \rangle = \begin{cases} \mathcal{F}_h & \text{on horizontal links} \\ \mathcal{F}_v & \text{on vertical links,} \end{cases}$$

$$\langle \mathcal{A}_{ij} \rangle = \begin{cases} \mathcal{A}_h & \text{on horizontal links} \\ \mathcal{A}_v & \text{on vertical links,} \end{cases}$$

$$\langle c_i^\dagger c_j \rangle = \begin{cases} \mathcal{C}_h & \text{on horizontal links} \\ \mathcal{C}_v & \text{on vertical links.} \end{cases} \quad (4)$$

Since the Hamiltonian does not involve \mathcal{A}_h , there are at this point six mean-field parameters.

The mean-field Hamiltonian, up to a constant, is then given by a sum of three terms:

$$\mathcal{H}_{\text{mf}} = \mathcal{H}_{\text{hop}} + \mathcal{H}_{\text{sw}} + \mathcal{H}_{\text{cond}},$$

with

$$\mathcal{H}_{\text{hop}} = -\frac{S}{2} t_h \mathcal{F}_h \sum_{\langle ij \rangle}^h (c_i^\dagger c_j + c_j^\dagger c_i) - \frac{S}{2} t_v \mathcal{F}_v (c_i^\dagger c_j + c_j^\dagger c_i) \quad (5)$$

and

$$\begin{aligned} \mathcal{H}_{\text{sw}} &= \Lambda \sum_{i\sigma} b_{i\sigma}^\dagger b_{i\sigma} + \frac{1}{2} (J_h \mathcal{F}_h - S t_h \mathcal{C}_h) \sum_{\langle ij \rangle}^h (\mathcal{F}_{ij}^\dagger + \mathcal{F}_{ij}) \\ &+ \frac{1}{2} \sum_{\langle ij \rangle}^v [J_v \mathcal{A}_v (\mathcal{A}_{ij}^\dagger + \mathcal{A}_{ij}) - S t_v \mathcal{C}_v (\mathcal{F}_{ij}^\dagger + \mathcal{F}_{ij})]. \end{aligned} \quad (6)$$

Here, $\sum_{\langle ij \rangle}^h$ and $\sum_{\langle ij \rangle}^v$ represent sums over horizontal and vertical links, respectively. In the sum over bonds, each bond occurs once, and vertical bonds $\langle ij \rangle$ always have i on even-numbered planes and j on odd-numbered planes.

To the hopping and spin-wave Hamiltonians $\mathcal{H}_{\text{hop}} + \mathcal{H}_{\text{sw}}$ we add a contribution from a field $B_{i\sigma}$ that couples linearly to the Schwinger boson field:

$$\mathcal{H}_{\text{cond}} = -\sqrt{N} \sum_{i\sigma} (B_{i\sigma}^* b_{i\sigma} + B_{i\sigma} b_{i\sigma}^*), \quad (7)$$

where N is the total number of lattice sites. The Fourier transform $B_{\mathbf{k}\sigma}$ is a field that is conjugate to the Schwinger boson condensate order parameter:

$$\Psi_{\mathbf{k}\sigma} \equiv \frac{1}{\sqrt{N}} \langle b_{\mathbf{k}\sigma}^\dagger \rangle = -\frac{1}{N} \left\langle \frac{\partial F}{\partial B_{\mathbf{k}\sigma}} \right\rangle, \quad (8)$$

where F is the free energy.

Diagonalizing \mathcal{H}_{sw} , we find

$$\begin{aligned} \mathcal{H}_{\text{sw}} &= \sum_{\mathbf{k}, \sigma} E(\mathbf{k}) \beta_{\mathbf{k}\sigma}^\dagger \beta_{\mathbf{k}\sigma} + \sum_{\mathbf{k}} (\sqrt{\Lambda_{\mathbf{k}}^2 - \Delta_{\mathbf{k}}^2} - \Lambda_{\mathbf{k}}) \\ &- N \sum_{\mathbf{k}} \begin{pmatrix} B_{\pi-\mathbf{k}\uparrow}^* & B_{\mathbf{k}\downarrow} \end{pmatrix} M^{-1}(\mathbf{k}) \begin{pmatrix} B_{\pi-\mathbf{k}\uparrow} \\ B_{\mathbf{k}\downarrow}^* \end{pmatrix} \end{aligned} \quad (9)$$

with $\boldsymbol{\pi} = (0, 0, \pi)$,

$$M(\mathbf{k}) = \begin{pmatrix} \Lambda_{\mathbf{k}} - \Omega_{\mathbf{k}} & \Delta_{\mathbf{k}} \\ \Delta_{\mathbf{k}} & \Lambda_{\mathbf{k}} + \Omega_{\mathbf{k}} \end{pmatrix},$$

and

$$\Lambda_{\mathbf{k}} = \Lambda - (J_h \mathcal{F}_h + S t_h \mathcal{C}_h) (\cos k_x + \cos k_y),$$

$$\Delta_{\mathbf{k}} = -J_v \mathcal{A}_v \cos k_z,$$

$$\Omega_{\mathbf{k}} = -S t_v \cos k_z,$$

$$E(\mathbf{k}) \equiv \sqrt{\Lambda_{\mathbf{k}}^2 - \Delta_{\mathbf{k}}^2} + \Omega_{\mathbf{k}}.$$

When there is a condensate ($T < T_c$) the Bose spectrum is gapless, with $\Lambda = \Lambda^*$, where

$$\Lambda^* \equiv 2(J_h \mathcal{F}_h + St_h \mathcal{C}_h) + \sqrt{(J_v \mathcal{A}_v)^2 + (St_v \mathcal{C}_v)^2}.$$

The dispersion then may be compared in the $x \rightarrow 0$ limit with the spin-wave result

$$E^{\text{sw}}(\mathbf{k}) = S \sqrt{[J_v + J_h(2 - \cos k_x - \cos k_y)]^2 - J_v^2 \cos^2 k_z},$$

obtained by expanding about a $(0,0,\pi)$ Néel state (alternating ferromagnetic planes). The basic functional dependence on \mathbf{k} is reproduced; this is a good preliminary check on the mean-field ansatz.

Note also the particle-hole symmetry present in our mean-field theory. This guarantees an $x \rightarrow 1-x$ symmetry in the phase diagram. As mentioned above, exchange in pure CaMnO_3 is different than in pure LaMnO_3 , due to the presence of the second set of empty e_g states. Hence, this symmetry is an artifact of our model.

In deriving the mean-field equations for our model, we must also include the condensate. The relationship between the field $B_{\mathbf{k}\sigma}$ and the order parameter $\Psi_{\mathbf{k}\sigma}$ is

$$\begin{pmatrix} \Psi_{\pi-\mathbf{k}\uparrow} \\ \Psi_{\mathbf{k}\downarrow}^* \end{pmatrix} = M^{-1}(\mathbf{k}) \begin{pmatrix} B_{\pi-\mathbf{k}\uparrow} \\ B_{\mathbf{k}\downarrow}^* \end{pmatrix}. \quad (10)$$

Differentiating the condensate contribution to the free energy with respect to a generic mean field parameter ξ gives

$$\frac{\partial F_{\text{cond}}}{\partial \xi} = N \sum_{\mathbf{k}} (\Psi_{\pi-\mathbf{k}\uparrow}^* \quad \Psi_{\mathbf{k}\downarrow}) \frac{\partial M(\mathbf{k})}{\partial \xi} \begin{pmatrix} \Psi_{\pi-\mathbf{k}\uparrow} \\ \Psi_{\mathbf{k}\downarrow}^* \end{pmatrix}.$$

Enacting a global $\text{SU}(2)$ rotation $b_{i\sigma} \rightarrow U_{\sigma\sigma'} b_{i\sigma'}$, it is easy to show that the free energy is invariant under such a transformation. This approach to Schwinger boson condensation can also be applied to the cases of the uniform ferromagnet or antiferromagnet. It has the comforting feature of making the $\text{SU}(2)$ invariance manifest from the outset (compare, e.g., with Ref. 14, in which the condensate always results in a moment in the x direction).

Proceeding in our analysis, we assume condensation only at $\mathbf{k}=0$ and $\mathbf{k}=\pi$. In order that the condensate give no contribution to the free energy, we require that

$$\begin{pmatrix} \Psi_{\pi\uparrow} \\ \Psi_{0\downarrow}^* \end{pmatrix} = -X e^{i\gamma} \begin{pmatrix} \cos \frac{1}{2} \vartheta \\ -\sin \frac{1}{2} \vartheta \end{pmatrix}, \quad (11)$$

$$\begin{pmatrix} -\Psi_{\pi\downarrow}^* \\ \Psi_{0\uparrow} \end{pmatrix} = -Y e^{i\delta} \begin{pmatrix} \cos \frac{1}{2} \vartheta \\ -\sin \frac{1}{2} \vartheta \end{pmatrix},$$

where

$$\tan \vartheta = \frac{J_v \mathcal{A}_v}{St_v \mathcal{C}_v}, \quad (12)$$

and X , Y , γ , and δ are at this point arbitrary parameters specifying the direction and magnitude of what is in general a canted $(0,0,\pi)$ antiferromagnet.⁴ Equation (11) also is con-

sistent with the free energy being a convex function of the order parameter $\Psi_{\mathbf{k}\sigma}$. The condensate is then spatially varying, with

$$\langle b_{i\sigma} \rangle = \Psi_{0\sigma} + \Psi_{\pi\sigma} e^{i\pi \cdot \mathbf{R}_i}. \quad (13)$$

The condensate contribution to the local magnetization $\langle \mathbf{S}_i \rangle$ is easily computed and ϑ is found to be the canting angle.

IV. MEAN-FIELD EQUATIONS

We now are in a position to write down the mean-field equations. We work in the grand canonical ensemble, introducing a chemical potential μ for the fermions. This introduces a seventh parameter, and we obtain the following seven equations:

$$2S = \int \frac{d^3k}{(2\pi)^3} \frac{\Lambda_{\mathbf{k}}}{\sqrt{\Lambda_{\mathbf{k}}^2 - \Delta_{\mathbf{k}}^2}} \coth\left(\frac{E(\mathbf{k})}{2k_B T}\right) + R^2 - 1,$$

$$\frac{\mathcal{A}_v}{J_v} = \int \frac{d^3k}{(2\pi)^3} \frac{\mathcal{A}_v \cos^2 k_z}{\sqrt{\Lambda_{\mathbf{k}}^2 - \Delta_{\mathbf{k}}^2}} \coth\left(\frac{E(\mathbf{k})}{2k_B T}\right) + \frac{\mathcal{A}_v R^2}{\sqrt{(J_v \mathcal{A}_v)^2 + (St_v \mathcal{C}_v)^2}},$$

$$\mathcal{F}_h = \int \frac{d^3k}{(2\pi)^3} \frac{(\cos k_x + \cos k_y) \Lambda_{\mathbf{k}}}{2\sqrt{\Lambda_{\mathbf{k}}^2 - \Delta_{\mathbf{k}}^2}} \coth\left(\frac{E(\mathbf{k})}{2k_B T}\right) + R^2,$$

$$\mathcal{F}_v = 2 \int \frac{d^3k}{(2\pi)^3} \frac{\cos k_z}{\exp\left(\frac{E(\mathbf{k})}{k_B T}\right) - 1} + \frac{St_v \mathcal{C}_v}{\sqrt{(J_v \mathcal{A}_v)^2 + (St_v \mathcal{C}_v)^2}}, \quad (14)$$

$$\mathcal{C}_h = \frac{1}{2} \int \frac{d^3k}{(2\pi)^3} \frac{\cos k_x + \cos k_y}{\exp\left(\frac{\epsilon(\mathbf{k}) - \mu}{k_B T}\right) + 1},$$

$$\mathcal{C}_v = \int \frac{d^3k}{(2\pi)^3} \frac{\cos k_z}{\exp\left(\frac{\epsilon(\mathbf{k}) - \mu}{k_B T}\right) + 1},$$

$$x = \int \frac{d^3k}{(2\pi)^3} \frac{1}{\exp\left(\frac{\epsilon(\mathbf{k}) - \mu}{k_B T}\right) + 1},$$

where $R = \sqrt{X^2 + Y^2}$ is the condensate amplitude, x is the hole concentration, and

$$\epsilon(\mathbf{k}) = -St_h \mathcal{F}_h (\cos k_x + \cos k_y) - St_v \mathcal{F}_v \cos k_z$$

is the fermion dispersion. The integrals are performed over the first Brillouin zone of the cubic lattice. There are seven mean-field equations corresponding to seven mean-field parameters. The parameters are

$$T < T_c: \quad \mathcal{A}_v, \mathcal{F}_h, \mathcal{F}_v, \mathcal{C}_h, \mathcal{C}_v, \mu, R \quad (\Lambda = \Lambda^*),$$

$$T > T_c: \quad \mathcal{A}_v, \mathcal{F}_h, \mathcal{F}_v, \mathcal{C}_h, \mathcal{C}_v, \mu, \Lambda \quad (R=0).$$

There are three ordered phases (i.e., with $R > 0$) of interest (where LRO means long-range order):

(I) antiferromagnet (LRO at π): $\mathcal{F}_v = C_v = 0$,

(II) canted (LRO at 0 and π): $\mathcal{A}_v, C_v = 0$,

(III) Ferromagnet (LRO at 0): $\mathcal{A}_v = 0$.

These phases were identified by de Gennes;⁴ we have also found evidence of phase separation below T_c (see also Refs. 22 and 23), as we shall describe below. The disordered ($R = 0$) states may also be classified:

(IV) 3d local magnetic order: $\mathcal{F}_v \neq 0, \mathcal{F}_h \neq 0$,

(V) 2d local magnetic order: $\mathcal{F}_v = C_v = 0, \mathcal{F}_h \neq 0$,

(VI) pure local: $\mathcal{A}_v = \mathcal{F}_v = \mathcal{F}_h = C_v = C_h = 0$.

Phase IV describes a standard paramagnetic system. At sufficiently high temperatures (phases V and VI), neighboring spins become totally uncorrelated; this is an artifact of the mean-field theory. In what follows we describe our analytical and numerical investigations of the phase diagram.

V. $T=0, S \rightarrow \infty$ LIMIT

Our mean-field equations simplify considerably in the limit of zero temperature and $S \rightarrow \infty$. We examine the three ordered ($\Lambda = \Lambda^*$, $R > 0$) phases,

(I) $\mathcal{A}_v = \mathcal{F}_h = 2S$, $\mathcal{F}_v = C_v = 0$,

(II) $\mathcal{F}_v = \sqrt{4S^2 - \mathcal{A}_v^2} = S t_v C_v / J_v$, $\mathcal{F}_v = \mathcal{F}_h = 2S$,

(III) $\mathcal{A}_v = 0$.

The canted phase II can smoothly interpolate between the π antiferromagnet I and the ferromagnet III, with ϑ going from $\frac{1}{2}\pi$ to 0. We start with the canted structure, solving the mean-field equation $\mathcal{F}_v = 2C_v / J_v$. We do this in the regime $x \ll 1$ by expanding the fermion dispersion relation

$$\epsilon(\mathbf{k}) = \epsilon(0) + S t_v \mathcal{F}_v (1 - \cos k_z) + \frac{1}{2} S t_h \mathcal{F}_h (k_x^2 + k_y^2) + \dots;$$

since $\mathcal{F}_v = 0$ is a possible solution, we keep the full c -axis dispersion. We find that the solution is characterized by the dimensionless parameter $r \equiv 8\pi J_v t_h / t_v^2$. For $r > 1$, the only solution has $\mathcal{F}_v = C_v = 0$, and we have antiferromagnetism at finite doping. However, experiments¹⁹ suggest $J_v \approx 0.58$ meV while spin-density functional calculations²⁰ suggest $t_v \approx 44$ meV (the physical hopping parameter is $S^2 t \approx 100$ meV). This gives $r \approx 0.33$, so the $r > 1$ regime is unphysical for $\text{La}_{1-x}\text{A}_x\text{MnO}_3$. The ground-state energy per site is found to be

$$\frac{E_{(I)}}{NS^2} = -2J_h - J_v - 4t_h x + 2\pi t_h x^2 + \dots \quad (15)$$

For $r < 1$, we have a solution with nonzero \mathcal{F}_v . We find

$$\frac{E_{(II)}}{NS^2} = -2J_h - J_v - 4t_h x + 2\pi g(r) t_h x^2 + \dots, \quad (16)$$

$$g(r) = \frac{\pi^2 r - \pi \alpha \sin^2 \alpha}{(\sin \alpha - \alpha \cos \alpha)^2},$$

where $\alpha(r) \in [0, \pi]$ is defined implicitly by the equation

$$\alpha - \sin \alpha \cos \alpha = \pi r. \quad (17)$$

We obtain $\mathcal{F}_v = x t_v / J_v + \mathcal{O}(x^2)$ in this regime. For $r < \frac{1}{2}$, $g(r) < 0$ and the coefficient of x^2 is negative, indicating phase separation. For $\frac{1}{2} < r < 1$, $g(r) > 0$ and there is a homogeneous, thermodynamically stable canted phase, originally identified by de Gennes.⁴ Our estimate $r \approx 0.33$ suggests that phase separation is likely.

Within the canted phase, as x increases from 0 to $\frac{1}{2}$, the canting angle decreases from $\vartheta = \frac{1}{2}\pi$ (π is long-range ordered LRO) to $\vartheta = 0$ (0 is long-range ordered LRO). The transition from canted to ferromagnetic order is continuous, occurring at a critical concentration x^* determined by the simultaneous solution of the two equations,

$$x^* = \int \frac{d^3 k}{(2\pi)^3} \Theta(\mu - \epsilon(\mathbf{k})),$$

$$\frac{2J_v}{t_v} = \int \frac{d^3 k}{(2\pi)^3} \cos k_z \Theta(\mu - \epsilon(\mathbf{k})), \quad (18)$$

in the two variables x^* and μ . For sufficiently large J_v , ϑ is nonzero even at half-filling and the system remains canted for all x .

It is interesting to note that the same regimes with the same critical values for the parameter r can be obtained by minimizing the mean-field energy in the manner proposed by de Gennes.⁴ Phase separation was already implicit in the calculations reported there.

VI. FINITE- T PHASES

To explore the finite-temperature phases of our model, we have solved the mean-field equations numerically using the MINPACK routine HYBRD.F. (To simplify matters, we assumed $J_v = J_h \equiv J$ and $t_v = t_h \equiv t$.) We found that there is often more than one solution to the mean-field equations; in such cases we computed the energy of each solution and identified the minimum total energy state. To compare with the analytical results of the previous section, we computed the energy versus concentration x for three different values of r , all at a temperature well below T_c (see Fig. 1). This verified our prediction of phase separation for $0 < r < \frac{1}{2}$.

In Figs. 2 and 3 we plot phase diagrams for $J/t = 0.01$ ($r = 0.251$) and $J/t = 0.03$ ($r = 0.754$), respectively. Regions are labeled I through VI corresponding to the six phases discussed above (recall that a condensate is present only in phases I, II, and III). We find that for $J/t = 0.01$ all of region II is unstable toward phase separation. For $J/t = 0.03$, we found a first-order line separating phases I and II from the disordered phases. This is so even at $x = 0$; the mean-field theory predicts a first-order transition from the $(0, 0, \pi)$ Néel state to a magnetically disordered state. This is perhaps a worrisome artifact of the mean-field theory. In addition, the

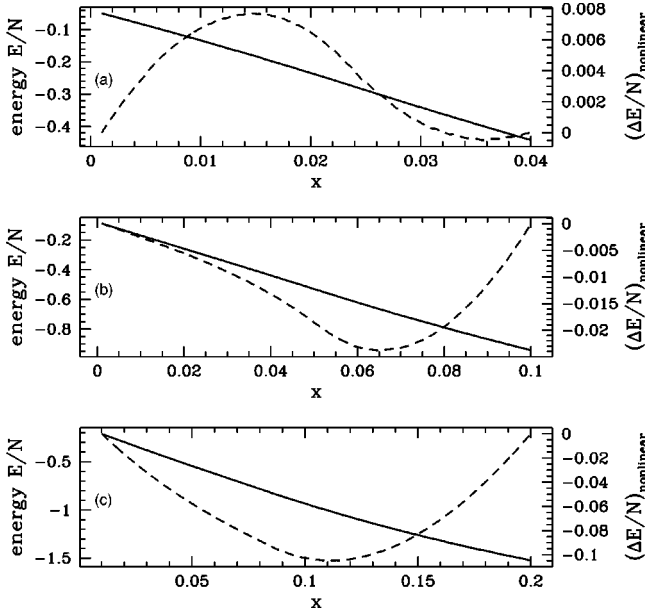


FIG. 1. Energy per site E/N (solid) versus concentration x for $J_v = J_h \equiv J$, $t_v = t_h \equiv t = 1$ at temperature $T = 0.01t$ for three different values of $r = 8\pi J/t$: (a) $r = 0.25$, (b) $r = 0.50$, (c) $r = 0.75$. To ascertain the sign of $\partial^2 E/\partial x^2$, we have subtracted from E/N the linear part; the dashed curve is the remaining contribution. Note that $E(x)$ is convex for small x in (a) and (b), indicative of phase separation.

transitions between the disordered phases may well become smooth crossovers when fluctuation effects are accounted for. Indeed, application of the Schwinger boson formalism to the Heisenberg model¹² leads to a spurious high-temperature mean-field transition to a state in which the magnon band-

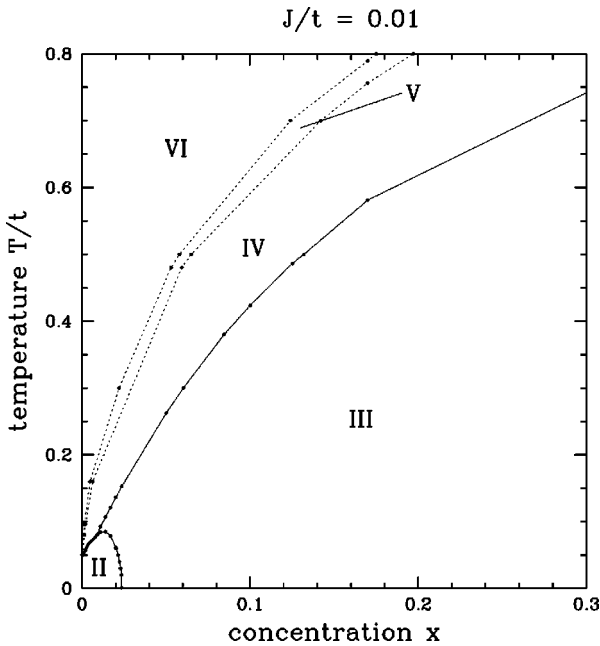


FIG. 2. Phase diagram for $J/t = 0.01$ ($r = 0.251$) obtained from numerical solution of the mean-field equations. The dark solid line separating phases II and IV is first order. All other transitions are second order. Dotted lines represent transitions between disordered states. Region II is phase separated.

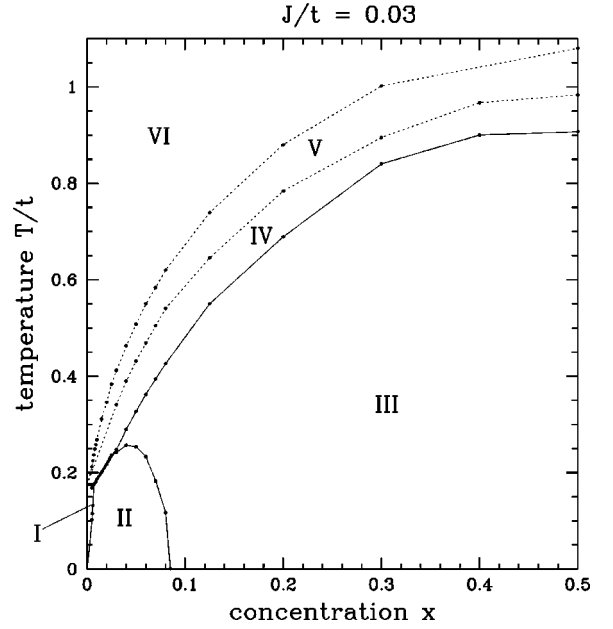


FIG. 3. Phase diagram for $J/t = 0.03$ ($r = 0.754$) obtained from numerical solution of the mean-field equations. A small sliver of the π -ordered phase exists in the lower left corner. The dark solid line separating phases I and IV as well as II and IV is first order. All other transitions are second order. As in Fig. 2, dotted lines represent transitions between disordered states.

width vanishes, analogous to phase (VI).

Sarker¹⁵ has discussed the behavior of the electron spectral function and found it to be entirely incoherent when the core spins are disordered. Writing (at finite-temperature T)

$$G_{\alpha\beta}^R(\mathbf{k}, t) = -i \langle \{ \psi_{\mathbf{k}\alpha}(t), \psi_{\mathbf{k}\beta}^\dagger(0) \} \rangle \Theta(t),$$

$$G_{\alpha\beta}^R(\mathbf{k}, \omega) = \int_{-\infty}^{\infty} d\omega' \frac{\rho_{\alpha\beta}(\mathbf{k}, \omega')}{\omega - \omega' + i0^+},$$

we find, at the mean-field level,

$$\rho_{\alpha\beta}(\mathbf{k}, \omega) = \int \frac{d^3 q}{(2\pi)^3} [n_{\alpha\beta}(\mathbf{q}) + \delta_{\alpha\beta} f(\mathbf{k} + \mathbf{q})] \times \delta(\omega + E(\mathbf{q}) - \epsilon(\mathbf{k} + \mathbf{q}) + \mu), \quad (19)$$

where $n_{\alpha\beta}(\mathbf{q}) = \langle b_{\mathbf{q}\alpha}^\dagger b_{\mathbf{q}\beta} \rangle$ and $f(\mathbf{p}) = \langle c_{\mathbf{p}}^\dagger c_{\mathbf{p}} \rangle$ are equilibrium averages. The contribution of the condensate to the spectral density results in well-defined quasiparticle peaks. For instance,

$$\rho_{\uparrow\uparrow}^{\text{cond}}(\mathbf{k}, \omega) = Y^2 \sin^2(\vartheta/2) \delta(\omega + E(0) - \epsilon(\mathbf{k}) + \mu) + X^2 \cos^2(\vartheta/2) \delta(\omega + E(\pi) - \epsilon(\pi - \mathbf{k}) + \mu),$$

where X , Y , and ϑ describe the amplitude and orientation of the condensate [recall Eq. (11)]. The remaining contribution to the spectral function $\Delta\rho$ is incoherent and spectrally broad.¹⁵ Our calculation allows for condensation both at $\mathbf{k} = 0$ as well as at $\mathbf{k} = \pi$, and as expected there are two quasiparticle peaks when translational symmetry is broken (phase I). A detailed study of $\rho(\mathbf{k}, \omega)$ in the various ordered and disordered phases is pending.

VII. CONCLUSIONS

We have shown that the double-exchange model has a variety of possible phase diagrams, controlled by the parameter $r \equiv 8\pi J_v t_h / t_v^2$. For realistic values of r , $0.05 \leq r \leq 0.2$, we find a phase diagram similar to the one proposed by de Gennes,⁴ except that the canted phase is replaced by a region of phase separation (note that this result can also be derived within the technique proposed there). In addition, the transition to the paramagnetic phase may be of first order, and the paramagnetic phase itself is anisotropic. For $r > \frac{1}{2}$, we find that the canted phase is stable. The main source of uncertainty in the value of r arises from the lack of a precise determination of the hoppings, which may depend on the composition and details of the lattice structure.³ Perhaps both situations may be realized experimentally.

Coulomb interactions will prevent charge separation at large scales. The electrostatic energy required to break the system into charged domains of side l goes as $e^2 x^2 / \epsilon l$, where ϵ is the dielectric constant. The magnetic energy cost to create a domain wall of size l is roughly $J_v (l/a)^2$, where a is the lattice spacing. Hence, the domain size, l goes as $a^{4/3} (J_v \epsilon / e^2 x^2)^{1/3}$, which should be on the order of a few lattice constants.

Phase separation in these compounds has previously been discussed phenomenologically in Ref. 22, and in Ref. 23, in the context of numerical results for the ferromagnetic Kondo lattice in one, two, and infinite dimensions. At large values

of the Hund's-rule coupling, this model reduces to the double-exchange model, plus antiferromagnetic interactions between the core spins. In-plane ferromagnetic interactions do not arise, as they are induced by the second e_g band. Our results, for $T=0$, are qualitatively in agreement with those reported in Ref. 23, provided that one identifies our canted phase with the incommensurate order reported there.

Our calculation reproduces the observed magnon spectrum at zero doping,¹⁸ except for a small anisotropy gap. In the canted phase, the long-wavelength spin waves behave as $\sqrt{v_{\parallel}(k_x^2 + k_y^2) + v_{\perp} k_z^2}$. In the phase-separated regime, localized ferromagnetic and antiferromagnetic modes are expected, which may have been observed experimentally.¹⁹

A detailed study of transport properties lies beyond the scope of the present calculation. It is interesting to note, however, that, in the presence of phase separation, hopping is suppressed in the out-of-plane direction in the antiferromagnetic domains. This effect can contribute to making these compounds insulating at low dopings, in agreement with experiments.^{24,25}

ACKNOWLEDGMENTS

We are particularly grateful to J. M. D. Coey for educating us on many issues regarding manganates. We also thank A. Millis for useful comments. F.G. acknowledges the hospitality of the University of California at San Diego, where this work was performed.

-
- ¹E. D. Wollan and W. C. Koehler, *Phys. Rev.* **100**, 545 (1955).
²See, e.g., J. B. Goodenough, *Magnetism and the Chemical Bond* (Interscience, New York, 1963).
³J. M. D. Coey, M. Viret, and S. von Molnar, *Adv. Phys.* (to be published).
⁴P.-G. de Gennes, *Phys. Rev.* **118**, 141 (1960).
⁵C. Zener, *Phys. Rev.* **82**, 403 (1951).
⁶H. Kawano, R. Kajimoto, M. Kubota, and H. Yoshizawa, *Phys. Rev. B* **53**, 2202 (1996).
⁷A. Asamitsu, Y. Moritomo, R. Kumai, Y. Tomioka, and Y. Tokura, *Phys. Rev. B* **54**, 1716 (1996).
⁸Y. Yamada, O. Hino, S. Nohdo, R. Kanao, T. Inami, and S. Katano, *Phys. Rev. Lett.* **77**, 904 (1996).
⁹J. W. Lynn, R. W. Erwin, J. A. Borchers, Q. Huang, A. Santoro, J. L. Peng, and Z. Y. Li, *Phys. Rev. Lett.* **76**, 4046 (1996).
¹⁰M. Viret, H. Glättli, C. Fermon, A. M. de Leon-Guevara, and A. Revcolevschi (unpublished).
¹¹A. Urushibara, Y. Moritomo, T. Arima, A. Asamitsu, G. Kido, and Y. Tokura, *Phys. Rev. B* **51**, 14 103 (1995).
¹²D. P. Arovas and A. Auerbach, *Phys. Rev. B* **38**, 316 (1988).
¹³A. J. Millis, P. B. Littlewood, and B. I. Shraiman, *Phys. Rev. Lett.* **74**, 5144 (1995).
¹⁴S. K. Sarker, C. Jayaprakash, H. R. Krishnamurty, and M. Ma, *Phys. Rev. B* **40**, 5028 (1989).
¹⁵S. K. Sarker, *J. Phys.: Condens. Matter* **8**, L515 (1996).
¹⁶C. M. Varma, *Phys. Rev. B* **54**, 7328 (1996).
¹⁷A. J. Millis, *Phys. Rev. B* **55**, 6405 (1997).
¹⁸F. Moussa, M. Hennion, J. Rodríguez-Carvajal, H. Moudden, L. Pinsard, and A. Revcolevschi, *Phys. Rev. B* **54**, 15 149 (1996).
¹⁹M. Hennion, F. Moussa, J. Rodríguez-Carvajal, L. Pinsard, and A. Revcolevschi, *Phys. Rev. B* **56**, R497 (1997).
²⁰W. E. Pickett and D. J. Singh, *Phys. Rev. B* **53**, 1146 (1996). In the ferromagnetic phase of $\text{La}_{2/3}\text{Ca}_{1/3}\text{MnO}_3$, these authors obtain a total (majority plus minority spins) density of states $\rho(E_F) \approx 0.85/\text{eV Mn}$. With $t_v = t_h \equiv t$, our bandwidth is $W = 12S^2 t$, and from $W\rho(E_F) \approx 1$ and $S = \frac{3}{2}$ we obtain $t \approx 44$ meV.
²¹We have scaled the hopping integrals by S^2 in order to allow a large- S analysis of our mean field equations.
²²E. L. Nagaev, *Usp. Fiz. Nauk* **166**, 833 (1996) [*Phys. Usp.* **39**, 781 (1996)]; E. L. Nagaev, *Physica B* **230-232**, 816 (1997).
²³J. Riera, K. Hallberg, and E. Dagotto, *Phys. Rev. Lett.* **79**, 713 (1997); E. Dagotto, S. Yunoki, A. L. Malvezzi, A. Moreo, J. Hu, S. Capponi, D. Poilblanc, and N. Furakawa, *Phys. Rev. B* **58**, 6414 (1998).
²⁴G. Allodi, R. de Renzi, G. Guidi, F. Licci, and M. W. Pieper, *Phys. Rev. B* **56**, 6036 (1997).
²⁵J.-S. Zhou, J. B. Goodenough, A. Asamitsu, and Y. Tokura, *Phys. Rev. Lett.* **79**, 3234 (1997).